Crystal structure, Hirshfeld surface analysis and computational study of the 1:2 co-crystal formed between N,N′-bis(pyridin-4-ylmethyl)ethane-diamide and 4-chlorobenzoic acid

Sang Loon Tan and Edward R. T. Tiekink*

Research Centre for Crystalline Materials, School of Science and Technology, Sunway University, 47500 Bandar Sunway, Selangor Darul Ehsan, Malaysia. *Correspondence e-mail: edwardt@sunway.edu.my

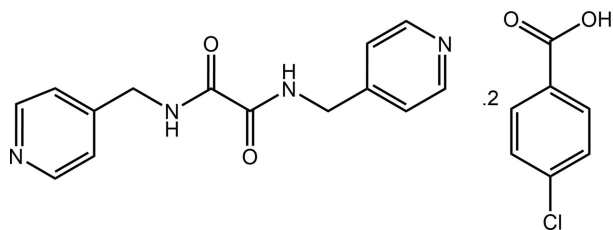The asymmetric unit of the title 1:2 co-crystal, $C_{14}H_{14}N_4O_2 \cdot 2C_7H_5ClO_2$, comprises two half molecules of oxalamide ($^4LH_2$), as each is disposed about a centre of inversion, and two molecules of 4-chlorobenzoic acid (CBA), each in general positions. Each $^4LH_2$ molecule has a (+)antiperiplanar conformation with the pyridin-4-yl residues lying to either side of the central, planar $C_2N_2O_2$ chromophore with the dihedral angles between the respective central core and the pyridyl rings being 68.65 (3) and 86.25 (3)°, respectively, representing the major difference between the independent $^4LH_2$ molecules. The anti conformation of the carbonyl groups enables the formation of intramolecular amide-N—H···O(amide) hydrogen bonds, each completing an $S(5)$ loop. The two independent CBA molecules are similar and exhibit C_6/CO_2 dihedral angles of 8.06 (10) and 17.24 (8)°, indicating twisted conformations. In the crystal, two independent, three-molecule aggregates are formed via carboxylic acid-O—H···N(pyridyl) hydrogen bonding. These are connected into a supramolecular tape propagating parallel to [100] through amide-N—H···O(amide) hydrogen bonding between the independent aggregates and ten-membered {···HNC₂O}₂ synthons. The tapes assemble into a three-dimensional architecture through pyridyl- and methylene-C—H···O(carbonyl) and CBA-C—H···O(amide) interactions. As revealed by a more detailed analysis of the molecular packing by calculating the Hirshfeld surfaces and computational chemistry, are the presence of attractive and dispersive Cl···C꞊O interactions which provide interaction energies approximately one-quarter of those provided by the amide-N—H···O(amide) hydrogen bonding sustaining the supramolecular tape.

1. Chemical context

This paper describes the X-ray crystal structure determination of, and an analysis of the supramolecular association in the 1:2 co-crystal formed between bis(pyridin-4-ylmethyl)ethanedi-amide and 4-chlorobenzoic acid, (I). The isomeric bis(pyridin-n-ylmethyl)ethanediamide molecules, i.e. molecules of the general formula $n\text{-}NC_5H_4CH_2N(H)C(꞊O)C(꞊O)CH_2\text{-}C_5H_4N\text{-}n$, for $n = 2$, 3 and 4, hereafter abbreviated as $^nLH_2$, are of interest as co-crystal co-formers owing to the presence of amide and pyridyl hydrogen bonding possibilities in their molecular structures (Tiekink, 2017). In a recent survey of co-crystals formed between $^4LH_2$ and carboxylic acids (Tan & Tiekink, 2020), the formation of carboxylic acid-O—H···N(pyridyl) hydrogen bonds in their co-crystals was reported to be universal with only one exception. The odd co-crystal was the 1:1 co-crystal formed between $^4LH_2$ and 2-[(4-hydroxyphenyl)diazenyl]benzoic acid (Arman et al., 2009).

245
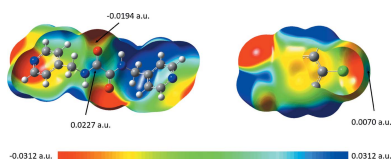
Within the acid, an intramolecular carboxylic acid-O—H···N(azo) hydrogen bond is instituted instead, leading to the formation of a $S(6)$ loop, an observation entirely in accord with expectation (Etter, 1990). The remaining co-crystal structures of ^4LH$_2$ with different carboxylic acids were stabilized by the expected carboxylic acid-O—H···N(pyridyl) hydrogen bonds, at both ends of the ^4LH$_2$ molecule. The formation of such O—H···N hydrogen bonding is consistent with literature precedent, which indicates a very high propensity for these hydrogen-bonding patterns between carboxylic acids and pyridyl entities, at least in the absence of competing supramolecular synthons (Shattock *et al.*, 2008). In only one case of co-crystallization experiments of ^4LH$_2$ with carboxylic acids was a salt formed owing to proton transfer, *i.e.* in the structure of [^4LH$_4$][2,6-dinitrobenzoate]$_2$, where pyridinium-N—H···O(carboxylate) hydrogen bonds are formed instead (Arman, Miller *et al.*, 2012). The title co-crystal, (I), was studied in continuation of on-going investigations of ^4LH$_2$ co-crystals of carboxylic acid co-formers (Arman *et al.*, 2012, 2013, 2014; Syed *et al.*, 2016; Tan, Halcovitch *et al.*, 2019; Tan & Tiekink, 2019).

2. Structural commentary

The crystallographic asymmetric unit of (I) comprises two half molecules of ^4LH$_2$, each being disposed about a centre of

Table 1
Hydrogen-bond geometry (Å, °).

D—H···A	D—H	H···A	D···A	D—H···A
N2—H2N···O1^i	0.88 (1)	2.35 (2)	2.7088 (14)	105 (1)
N4—H4N···O2^{ii}	0.87 (1)	2.30 (2)	2.7028 (14)	108 (1)
O4—H4O···N1	0.85 (2)	1.82 (2)	2.6559 (15)	171 (2)
O6—H6O···N3	0.85 (2)	1.80 (2)	2.6419 (15)	172 (2)
C8—H8···O5	0.95	2.53	3.1708 (17)	125
N2—H2N···O2^{iii}	0.88 (1)	2.11 (1)	2.8800 (13)	146 (1)
N4—H4N···O1	0.87 (1)	2.07 (1)	2.7959 (13)	141 (1)
C2—H2···O3^{iv}	0.95	2.53	3.3597 (17)	146
C6—H6A···O3^{iv}	0.99	2.59	3.5262 (17)	157
C9—H9···O5^v	0.95	2.59	3.3701 (17)	140
C13—H13A···O5^v	0.99	2.48	3.4006 (16)	155
C27—H27···O1^{vi}	0.95	2.53	3.4505 (16)	163

Symmetry codes: (i) $-x+1, -y+2, -z$; (ii) $-x+2, -y+2, -z$; (iii) $x-1, y, z$; (iv) $-x, -y+2, -z+1$; (v) $-x+1, -y+2, -z+1$; (vi) $-x+1, -y+1, -z+1$.

inversion, and two molecules of 4-chlorobenzoic acid (CBA), each in a general position. Pairs of ^4LH$_2$ and CBA molecules are connected *via* carboxylic acid-O—H···N(pyridyl) hydrogen bonding, Table 1, and with the application of symmetry, two independent, three-molecule aggregates eventuate, *i.e.* ^4LH$_2$(CBA)$_2$, as shown in Fig. 1.

As each ^4LH$_2$ molecule is centrosymmetric, the central C$_2$N$_2$O$_2$ chromophore in each is strictly planar. As is usually found in these molecules (Tiekink, 2017; Tan & Tiekink, 2020), the central C7—C7^i [1.537 (2) Å] and C14—C14^{ii} [1.539 (2) Å] bond lengths are longer than usual owing to the electronegative substituents connected to both carbon atoms [symmetry operations (i) $1-x, 2-y, -z$ and (ii) $2-x, 2-y, -z$]. The conformation of each ^4LH$_2$ molecule is (+)antiperiplanar whereby the pyridin-4-yl residues lie to either side of the planar region of the molecule. The dihedral angles between the respective central core and the N1- and N3-pyridyl rings are 68.65 (3) and 86.25 (3)°, respectively. This represents the greatest conformational difference between the ^4LH$_2$ molecules and is emphasized in the overlay diagram of Fig. 2 which shows the two independent, three-molecule aggregates. Finally, the carbonyl groups are *anti*, enabling the formation of intramolecular amide-N—H···O(amide) hydrogen bonds that complete $S(5)$ loops, Table 1.

To a first approximation, the two independent CBA molecules in (I) are similar. The dihedral angle between the benzene ring and the attached CO$_2$ group is 8.06 (10)° for the O3-molecule indicating a closer to co-planar molecule than for the O5-molecule for which the equivalent dihedral angle is 17.24 (8)°. Consistent with the carboxylic acid assignment, the C15—O3(carbonyl) bond length of 1.2172 (17) Å is consider-
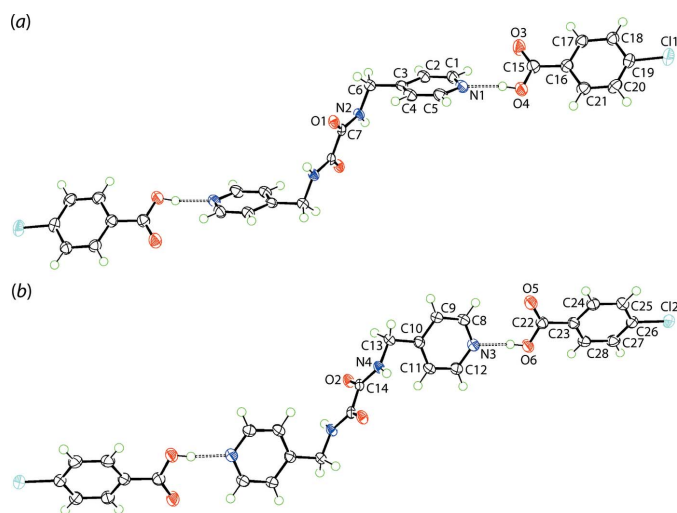

Figure 1
The molecular structures of the two centrosymmetric three-molecule aggregates in the crystal of (I) showing the atom-labelling scheme and displacement ellipsoids at the 70% probability level. In (*a*), the unlabelled atoms are related by the symmetry operation (i) $1-x, 2-y, -z$ and in (*b*), by (ii) $2-x, 2-y, -z$.
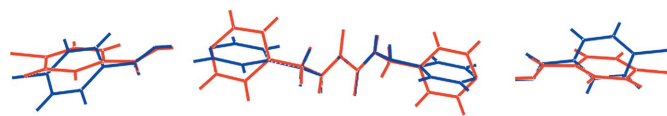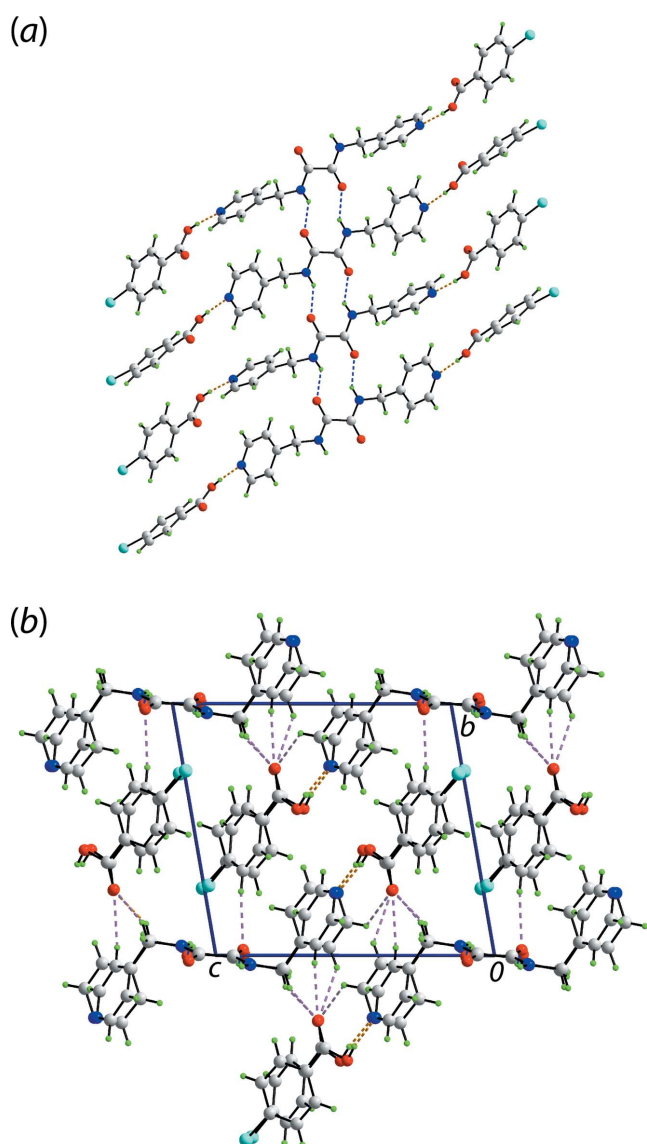

Figure 2
An overlay diagram of the two independent, three-molecule aggregates in (I). The N1-pyridyl/O3-carboxylic acid (red image) and N3-pyridyl/O5-carboxylic acid (blue image) aggregates have been overlapped so that the central C$_2$N$_2$O$_2$ chromophores are coincident.

ably shorter than the C15—O4(hydroxy) bond of 1.3196 (16) Å; the bonds of the O5-benzoic acid follow the same trend with C22—O5 of 1.2173 (17) Å compared with C22—O6 of 1.3181 (16) Å. As seen from Fig. 2, the attached benzoic acid molecules are each twisted out of the plane through the pyridyl ring they are connected to as seen in the N1-pyridyl/O3-carboxylic acid dihedral angle of 41.70 (4)°; the corresponding angle for the second three-molecule aggregate is 35.47 (3)°.

3. Supramolecular features

The formation of two independent, three-molecule aggregates has already been noted above in the crystal of (I) as has the

(a)

(b)

Figure 3
Molecular packing in the crystal of (I): (a) supramolecular tape comprising three-molecule aggregates, each sustained by carboxylic acid-O—H···N(pyridyl) hydrogen bonding (orange dashed lines), linked by amide-N—H···O(amide) (blue dashed lines) hydrogen bonding and (b) a view of the unit-cell contents down the a axis with C—H···O interactions highlighted by pink dashed lines.

Table 2
A summary of short interatomic contacts (Å) in (I)[a].

| Contact	Distance	Symmetry operation
O5···H9	2.49	$1 - x, 2 - y, 1 - z$
O5···H13A	2.40	$1 - x, 2 - y, 1 - z$
Cl2···C14	3.21	$-1 + x, -1 + y, 1 + z$
Cl2···O2	3.22	$-1 + x, -1 + y, 1 + z$
O1···H27	2.92	$1 - x, 1 - y, 1 - z$
O1···H4N[b]	1.96	x, y, z
O2···H2N[b]	2.00	$-1 + x, y, z$
O5···H8	2.46	x, y, z
N3···H6O[b]	1.67	x, y, z
O3···H2	2.42	$1 - x, 2 - y, 1 - z$
O3···H6A	2.51	$1 - x, 2 - y, 1 - z$
C7···Cl1	3.25	$x, 1 + y, -1 + z$
N1···H4O[b]	1.68	$-1 + x, y, z$
O3···H1	2.60	$-1 + x, y, z$
O1···Cl1	3.24	$x, 1 + y, -1 + z$

Notes: (a) The interatomic distances are calculated in *Crystal Explorer 17* (Turner *et al.*, 2017) whereby the X—H bond lengths are adjusted to their neutron values; (b) these interactions correspond to conventional hydrogen bonds.

intramolecular amide-N—H···O(amide) hydrogen bonds, Table 1. The carboxylic acid-O—H···N(pyridyl) hydrogen bond involving the O5-carboxylic acid and N3-pyridyl ring is supported by a pyridyl-NC—H···O(carbonyl) contact which closes a seven-membered {···OCOH···NCH} pseudo-heterosynthon; the corresponding H···O separation for the O3-carboxylic acid and N1-pyridyl ring is 2.67 Å. The three-molecule aggregates are connected into a supramolecular tape along the a axis by amide-N—H···O(amide) hydrogen bonding and concatenated, centrosymmetric 10-membered {···HNC$_2$O}$_2$ synthons, Fig. 3(a). The tapes are consolidated into a three-dimensional architecture by pyridyl- and methylene-C—H···O(carbonyl) and CBA-C—H···O(amide) interactions, Fig. 3(b).

4. Hirshfeld surface analysis

The calculation of the Hirshfeld surfaces and two-dimensional fingerprint plots were accomplished with the program *Crystal Explorer 17* (Turner *et al.*, 2017) using procedures described in the literature (Tan, Jotani *et al.*, 2019; Jotani *et al.*, 2019). The input for the calculations were the two independent three-molecule aggregates, hereafter 3M-I and 3M-II, shown in Fig. 2, whereby two chlorobenzoic acid (CBA) molecules are connected to each $^4LH_2$ molecule *via* carboxylic acid-O—H···N(pyridyl) hydrogen bonds. Analogous calculations were also performed on the symmetry expanded N1- and N3-oxalamide molecules, hereafter $^4LH_2$-I and $^4LH_2$-II, respectively, and on the independent O3- and O5-chlorobenzoic acid molecules, hereafter CBA-I and CBA-II, respectively. The d_{norm} distances for short contacts identified through the Hirshfeld surface analysis are given in Table 2.

Several d_{norm} maps showing red spots ranging from moderate to strong intensity are illustrated in Fig. 4. In particular, intense red spots indicative of strong interactions (Spackman & Jayatilaka, 2009) are observed for carboxylic-O4—H4O···N1(pyridyl) in 3M-I, carboxylic-O6–H6O···
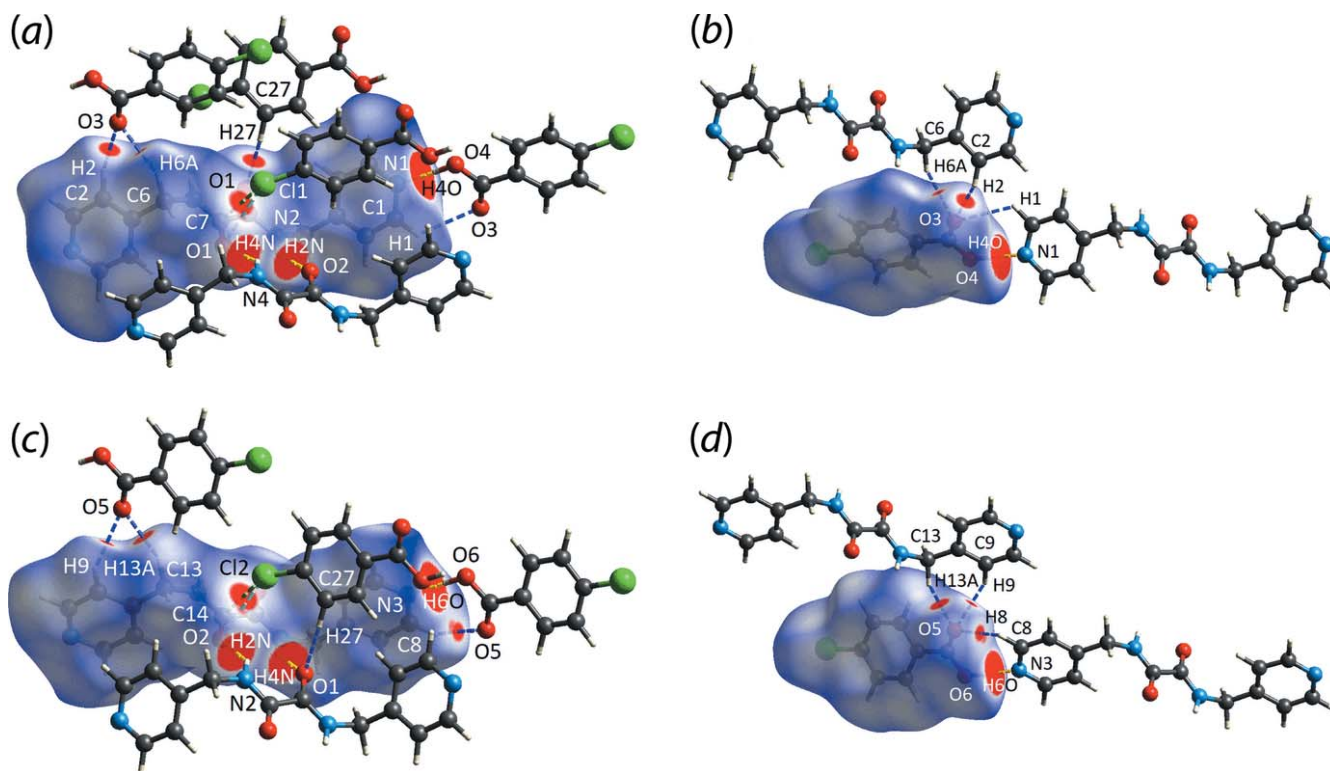
Figure 4
The d_{norm} maps showing N—H⋯O (yellow dashed lines), C—H⋯O (blue), Cl⋯C (green) and Cl⋯O (light-blue) close contacts as indicated by the corresponding red spots with varying intensities within the range of −0.0503 to 1.1157 arbitrary units for (a) [4]LH₂-I, (b) CBA-I, (c) [4]LH₂-II and (d) CBA-II.
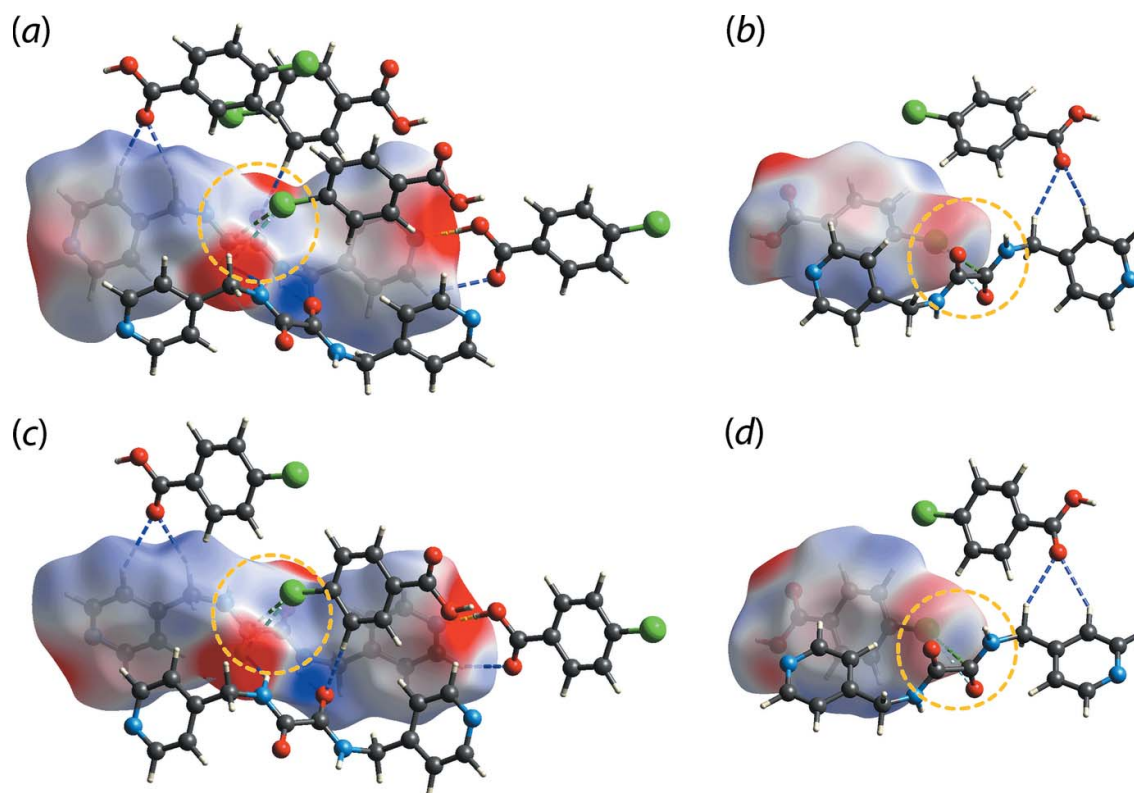
Figure 5
The electrostatic potential mapped onto the Hirshfeld surfaces within the isosurface value of −0.0416 to 0.0981 atomic units for (a) [4]LH₂-I, (b) CBA-I, (c) [4]LH₂-II and (d) CBA-II. The circles highlight the interactions between the electronegative sites of the amide and the chlorine atoms through the electropositive σ-hole region.
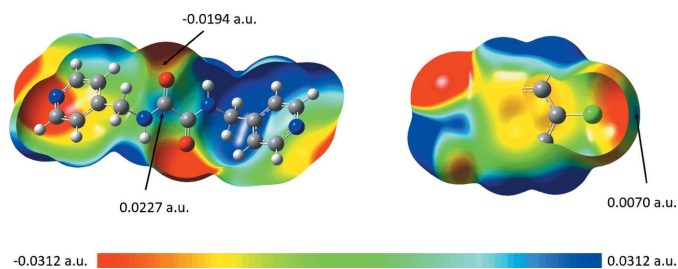
Figure 6
The electrostatic potential surface mapping for $^4LH_2$ and CBA as obtained from *Gaussian 16*, showing the average ESP charge on the surface of the point of contact for the Cl1/Cl2, C7/C14 and O1/O2 interactions. The electrostatic potential was mapped onto the isodensity surface (0.0004 a.u.) within the scale of −0.0312 to 0.0312 a.u.

N3(pyridyl) in 3M-II as well as the interactions between amide-N2—H2N···O2(amide) and amide-N4—H4N···O1(amide) in 3M-I and 3M-II, respectively, while relatively weaker interactions with moderately to weakly intense red spots between amide-C7···Cl1, pyridyl-C1—H1···O3(carboxylic acid), pyridyl-C2—H2···O3(carboxylic acid), methylene-C—H6A···O3(carboxylic acid), amide-O1···Cl1 in 3M-I, and Cl2···C14(amide), methylene-C13—H13A···O5(carboxylic acid), pyridyl-C8—H8···O5(carboxylic acid), pyridyl-C9—H9···O5(carboxylic acid), Cl2···O2(amide) in 3M-II are observed. As well, spots due to benzene-C27—H27···O1(amide) are seen, *i.e.* providing connections between 3M-I and 3M-II.

Qualitatively, the d_{norm} maps for 3M-I and 3M-II exhibit similarity for the corresponding $^4LH_2$ and CBA molecules with the exception of CBA-II. Pairs of CBA-II are aligned around an inversion centre with Cl2 and H25 being directly opposite each other, ostensibly forming an eight-membered heterosynthon despite the distance being longer than the cut-off value of 2.84 Å (Spek, 2020); such an alignment is not observed for CBA-I. In addition, there are other close contacts: C1—H1···O3, C6—H6A···O3, C7···Cl1, Cl2···C14, O1···Cl1 and Cl2···O2, which were not identified in the *PLATON* (Spek, 2020) analysis.

To establish the nature of the intermolecular interactions, particularly for the weaker contacts, a mapping of the electrostatic potential (ESP) was performed over the Hirshfeld surfaces through DFT-B3LYP/6-31G(d,p) for the independent $^4LH_2$ and CBA molecules in (I), Fig. 5. The results indicate the C1—H1···O3, C6—H6A···O3, C7···Cl1, Cl2···C14, O1···Cl1 and Cl2···O2 contacts are indeed electrostatic in nature, as shown from the red (electronegative) and blue (electropositive) regions on the ESP maps despite being relatively less intense when compared to those arising from the classical hydrogen bonds.

ESP calculations were also performed on the individual molecules through *Gaussian 16* (Frisch *et al.*, 2016) using the long-range corrected wB97XD density functional with Grimme's D2 dispersion density functional theoretical model (Chai & Head-Gordon, 2008) coupled with Pople's 6-311+G(d,p) basis set (Petersson *et al.*, 1988) in order to validate the above

results. The calculations show that the individual $^4LH_2$ and CBA molecules possess similar electrostatic surface potentials with the red and blue regions representing the extremities of the electrostatic potential spectrum, Fig. 6.

Of particular interest is the observation that the chlorine atom interacts with the amide-C=O residue through an electron-deficient σ-hole region. To complement the ESP findings on these O···Cl and C···Cl contacts, non-covalent interaction plots were generated for the relevant pairwise molecules using *NCIPLOT* (Johnson *et al.*, 2010). The results, as shown from the green domain on the isosurface between the $^4LH_2$ and CBA molecules in Fig. 7, indicate that those interactions are weakly attractive (Contreras-García *et al.*, 2011). The calculated electrostatic potential charge on the
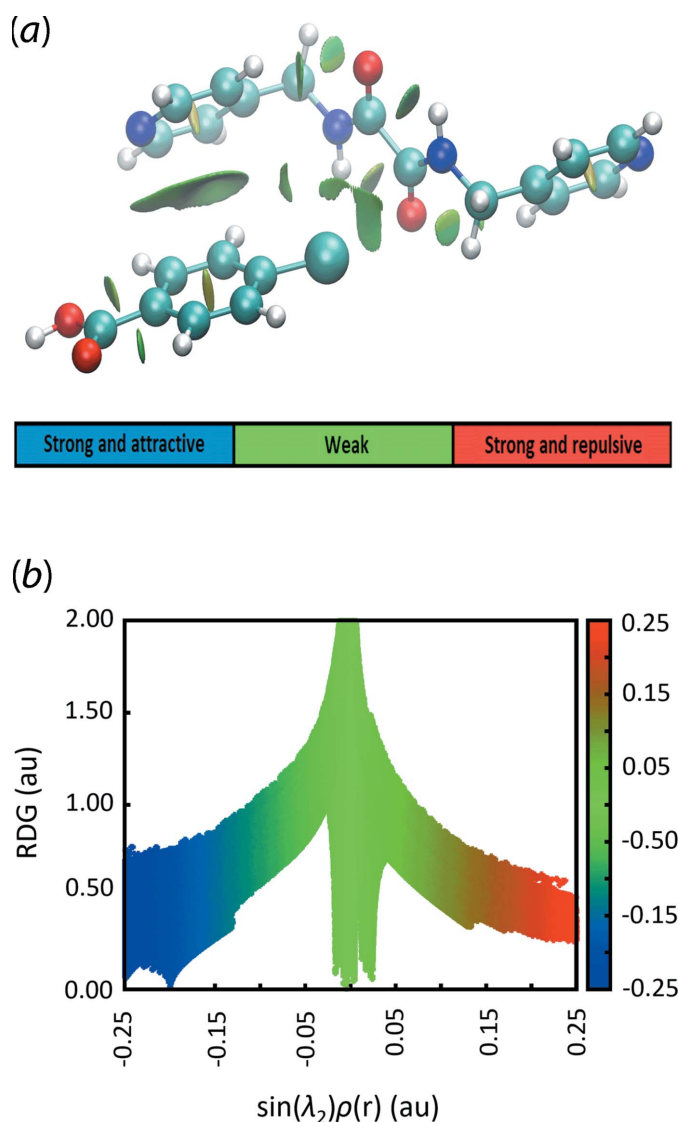
Figure 7
(*a*) The NCI plot highlighting the O···Cl and C···Cl contacts between $^4LH_2$-I and CBA-I molecules, showing the weak, but attractive interactions through the green domain and (*b*) the two-dimensional reduced density gradient versus the electron density times the sign of the second Hessian eigenvalue which reveals the overall contact profile of the pairwise molecules. The gradient cut-off is set at 0.4 and the colour scale is $−0.25 < \rho < 0.25$ a.u.
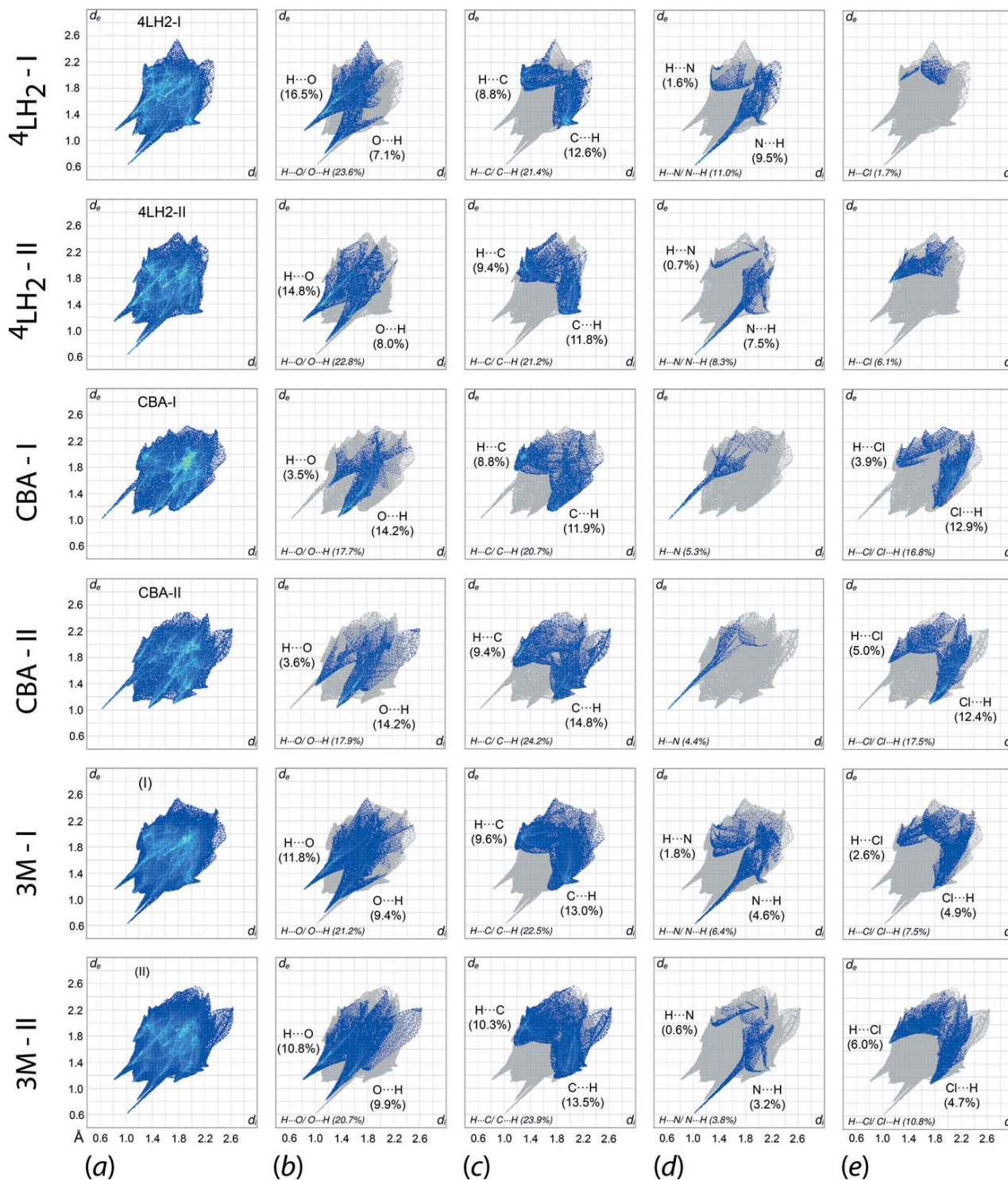
Figure 8
(a) The overall two-dimensional fingerprint plots for $^4LH_2$-I, $^4LH_2$-II, CBA-I, CBA-II, 3M-I and 3M-II, and those delineated into (b) H···O/O···H, (c) H···N/N···H, (d) H···C/C···H and (e) H···Cl/Cl···H contacts, with the percentage contributions specified within each plot.

surface at the point of contacts calculated with *Crystal Explorer 17* employing B3LYP/6-31G(*d,p*) are comparable to the data obtained from *Gaussian 16*, in which Cl1, O1, Cl2 and O2 possess charges of +0.0054, −0.0147, +0.0054 and −0.0125 atomic units (a.u.), respectively; while the C7 and C14 atoms each exhibit a weak electrostatic potential charge of +0.0251

and +0.0263 a.u., respectively. Therefore, the C7···Cl1 and C14···Cl2 interactions are dispersive in nature. On the other hand, the apparent charge complementarity between the Cl2 and H25 atoms, which align around a centre of inversion as described above, indicate the existence of an electrostatic interaction between two CBA-II molecules, Fig. 5(*d*).

Table 3
A summary of interaction energies (kJ mol^1) calculated for (I).

Contact	E_{ele}	E_{pol}	E_{dis}	E_{rep}	E_{tot}	Symmetry operation
N2—H2$N\cdots$O2/						
N4—H4$N\cdots$O1	−51.0	−12.4	−49.4	71.6	−61.9	x, y, z
O4—H4$O\cdots$N1/						
C1—H1$\cdots$O3	−84.3	−20.1	−12.7	106.3	−49.4	$−1 + x, y, z$
O6—H6$O\cdots$N3/						
C8—H8$\cdots$O5	−90.9	−21.4	−13.1	115.6	−52.0	x, y, z
C7$\cdots$Cl1/ O1$\cdots$Cl1	−5.3	−1.0	−25.4	19.3	−16.6	$x, 1 + y, −1 + z$
C6—H6$A\cdots$O3/						
C2—H2$\cdots$O3	−11.9	−3.2	−12.5	16.5	−15.8	$1 − x, 2 − y, 1 − z$
C9—H9$\cdots$O5/						
C13—H13$A\cdots$O5	−12.8	−3.6	−13.3	18.5	−16.3	$1 − x, 2 − y, 1 − z$
C14$\cdots$Cl2/ O2$\cdots$Cl2	−6.6	−0.8	−27.3	27.2	−14.5	$−1 + x, −1 + y, 1 + z$
C25—H25$\cdots$Cl2	−6.4	−0.7	−13.5	16.7	−8.7	$−x, − y, − z$
C27—H27$\cdots$O1	−10.4	−1.6	−23.4	19.7	−20.4	$1 − x, 1 − y, 1 − z$

The two-dimensional fingerprint plots were generated in order to quantify the close contacts for ^4LH$_2$-I, ^4LH$_2$-II, CBA-I, CBA-II, 3M-I and 3M-II. The overall fingerprint plots for the specified molecules/aggregates are shown in Fig. 8(a) and those decomposed into H$\cdots$O/O$\cdots$H/ H$\cdots$C/C$\cdots$H, H$\cdots$N/N$\cdots$H and H$\cdots$Cl/Cl$\cdots$H plots are shown in Fig. 8(b)-(e).

The overall fingerprint plot of the individual components and the corresponding three-molecule aggregates exhibit a paw-like profile with asymmetric spikes indicating the interdependency of the intermolecular interactions between molecules to sustain the packing. The 3M-I and 3M-II aggregates display almost identical fingerprint profiles which, upon decomposition, can be delineated into H$\cdots$H [32.5% for 3M-I and 30.1% for 3M-II; not illustrated], H$\cdots$C/C$\cdots$H [22.5 and 23.9%, respectively], H$\cdots$O/O$\cdots$H [21.2 and 20.7%], H$\cdots$Cl/Cl$\cdots$H [7.5 and 10.8%], H$\cdots$N/N$\cdots$H [6.4 and 3.8%] and other minor contacts [10.0 and 10.7%]. A detailed analysis on the corresponding decomposed fingerprint plots shows that only the H$\cdots$O/O$\cdots$H and H$\cdots$N/N$\cdots$H contacts for both 3M-I and 3M-II as well as H$\cdots$Cl/Cl$\cdots$H for 3M-II have $d_i + d_e$ distances shorter than the sum of the respective van der Waals radii of 2.61, 2.64 and 2.84 Å (adjusted to neutron values). For 3M-I, the $d_i + d_e$ values for the H$\cdots$O/O$\cdots$H and H$\cdots$N contacts are, respectively, tipped at ~1.98, ~1.95 and ~1.68 Å, and are attributed to (internal)-N2—H2$N\cdots$O2-(external), (internal)-O1$\cdots$H4N-(external) and (internal)-N1$\cdots$H4O-(external) contacts, respectively. The analogous contacts for 3M-II are tipped at 1.95 Å for (internal)-H4$N\cdots$O1-(external), ~1.98 Å for (internal)-O2$\cdots$H2N-(external) and ~1.64 Å for (internal)-N3$\cdots$H6O-(external). For H$\cdots$Cl/Cl$\cdots$H in 3M-II, the contacts are each tipped at ~2.80 Å owing to the pair of (internal)-H25$\cdots$Cl2-(external) and (internal)-Cl2$\cdots$H25-(external) interactions. As for the H$\cdots$H and H$\cdots$C/ C$\cdots$H contacts, their $d_i + d_e$ distances are longer than the sum of their respective van der Waals radii of 2.18 and 2.79 Å, and hence contribute little to the overall packing of the crystal despite providing the predominant surface contacts.

The individual ^4LH$_2$-I and ^4LH$_2$-II molecules exhibit similar fingerprint profiles with only slight differences in the contact distributions. In order of dominance, these are H$\cdots$H (36.3% for ^4LH$_2$-I and 33.8% for ^4LH$_2$-II), H$\cdots$O/O$\cdots$H (23.6 and 22.8%, respectively), H$\cdots$C/C$\cdots$H (21.4 and 21.2%), H$\cdots$N/N$\cdots$H (11.0 and 8.3%), H$\cdots$Cl (1.7 and 6.1%) and other minor contacts (6.0 and 7.8%). There is no major deviations in the $d_i + d_e$ distances cf. 3M-1 and 3M-II, with only the H$\cdots$O/O$\cdots$H as well as N$\cdots$H contacts being shorter than the sums of their respective van der Waals radii. Each of ^4LH$_2$-I and ^4LH$_2$-II have $d_i + d_e$ of about 1.98 Å for H$\cdots$O/O$\cdots$H and ~1.64 Å for N$\cdots$H contacts.

As for the individual CBA-I and CBA-II molecules, major contacts comprise H$\cdots$H (23.7% for CBA-I and 22.1% for CBA-II), H$\cdots$C/C$\cdots$H (20.7 and 24.2%, respectively), H$\cdots$O/O$\cdots$H (17.7 and 17.9%), H$\cdots$Cl/Cl$\cdots$H (16.8 and 17.5%), H$\cdots$N (5.3 and 4.4%) and other minor contacts (15.7 and 13.9%). A detailed analysis of the corresponding contacts shows all major interactions for CBA-I and CBA-II are more inclined toward (internal)-$X\cdots$H-(external) rather than (internal)-H$\cdots X$-(external), as evidenced most notably from the distribution for O$\cdots$H (CBA-I: 14.2%; CBA-II: 14.2%) versus H$\cdots$O (CBA-I: 3.5%; CBA-II: 3.6%) and Cl$\cdots$H (CBA-I: 12.9%; CBA-II: 12.4%) vs H$\cdots$Cl (CBA-I: 3.9%; CBA-II: 5.0%). The inclination arises due to the lack of hydrogen-bond donor atoms in the CBA-I and CBA-II molecules, other than the carboxylic acid groups, so they act primarily as hydrogen-bond acceptors. Among the contacts, O$\cdots$H and H$\cdots$N for CBA-I have $d_i + d_e$ distances of ~2.40 and ~1.64 Å, respectively, each being shorter than the sum of the respective van der Waals radii, while the same is true for H$\cdots$O/O$\cdots$H, H$\cdots$N and H$\cdots$Cl/Cl$\cdots$H contact for CBA-II with $d_i + d_e$ distances of ~2.38, ~1.62 and ~2.82 Å, respectively.

5. Computational chemistry

The calculation of the interaction energies for all pairwise interacting molecules was performed through *Crystal Explorer 17* (Turner *et al.*, 2017) based on the method reported previously (Tan, Jotani *et al.*, 2019) in order to study the strength of each interaction identified from the Hirshfeld surface analysis. The calculations showed that the ten-membered synthons formed between ^4LH$_2$-I and ^4LH$_2$-II

through amide-N2—H2N···O2(amide) and amide-N4—H4N···O1(amide) hydrogen bonds has the greatest energy among all close contacts present in the crystal with an interaction energy (E_{int}) of −61.9 kJ mol^{-1}. This is followed by the seven-membered heterosynthon formed between $^4LH_2$-II and CBA-II through the carboxylic acid-O4—H4O···N1(pyridyl) hydrogen bond with the supporting pyridyl-C—H8···O5(carbonyl) contact so that E_{int} = −52.0 kJ mol^{-1}. For the analogous contact between $^4LH_2$-I and CBA-I but lacking the supporting pyridyl-C—H···O5(carbonyl) contact, it is gratifying to note the interaction energy is correspondingly less, *i.e.* E_{int} = −49.4 kJ mol^{-1}. The interactions between amide-C7···Cl1 and amide-O1···Cl1, summing to E_{int} of −16.6 kJ mol^{-1}, are also significant, as are the interactions between methylene-C–H6A···O3(amide) and pyridyl-C2–H2···O3(amide) with E_{int} = −15.8 kJ mol^{-1}. The equivalent interactions surrounding the $^4LH_2$-II molecule follow the same trends and give similar energies, Table 3. The benzoic-C25—H25···Cl2 dimer arising from the connection between two CBA-II molecules is weakly interacting with E_{int} of −8.7 kJ mol^{-1}. Finally, the C27—H27···O1(amide) interaction exhibits an E_{int} of −20.4 kJ mol^{-1}.

The crystal of (I) is mainly governed by electrostatic forces (E_{ele}) as highlighted by the rod-shaped energy framework with a zigzag topology due to the combination of several strong interactions, Fig. 9(a). Specifically, the combination of interactions between $^4LH_2$-I and CBA-I through the terminal O4—H4O···N1 hydrogen bonding as well as between $^4LH_2$-II and CBA-II *via* O6—H6O···N3 and C8—H8···O5 interactions leads to the formation of the core framework parallel to (101). The overall E_{ele} of these interactions is much greater than that associated with the ten-membered synthons formed by a combination of N2—H2N···O2 and N4—H4N···O1 hydrogen bonds as evidenced from the relatively small rod

radius in the energy model of the latter interactions, which align in a parallel fashion along the *b* axis, Fig. 9(a).

Apart from the electrostatic forces, the crystal is also sustained by substantial dispersion forces, which are mainly associated with the ten-membered {···HNC$_2$O}$_2$ synthon along with the peripheral C7···Cl1/O1···Cl1 and C14···Cl2/O2···Cl2 interactions which lead to a ladder-like topology, Fig. 9(b). The combination of the electrostatic and dispersion forces results in an enhancement of the influence of the ten-membered synthons which supersedes the energy force for the terminal carboxylic acid-O—H···N(pyridyl) hydrogen bonds as seen in the total energy framework, Fig. 9(c).

6. Database survey

The formation of carboxylic acid-O—H···N(pyridyl) hydrogen bonds, involving both pyridyl rings, leading to three-molecule aggregates, is an almost universal trait when co-crystals are formed between $^4LH_2$ and mono-functional carboxylic acids; one exception was noted in the *Chemical context*. A different situation pertains when bi-functional carboxylic acids are employed in co-crystal formation. In these circumstances, *e.g.* when the carboxylic acid is bis(carboxymethyl)urea and diglycineoxamide (Nguyen *et al.*, 2001), two-dimensional sheets result, owing to strands of {···HO$_2$C-R-CO$_2$H···$^4LH_2$···HO$_2$C-R-CO$_2$H···}$_n$ being connected by almost orthogonal tapes comprising ten-membered {···HNC$_2$O}$_2$ synthons provided by the $^4LH_2$ molecules. These are reinforced by hydrogen bonding afforded by the R residues of the bi-functional carboxylic acids, *e.g.* linked by six-membered synthons {···HNCNH···O} provided by the urea bridges in the case of bis(carboxymethyl)urea (Nguyen *et al.*, 2001). Clearly, scope remains for the development of novel
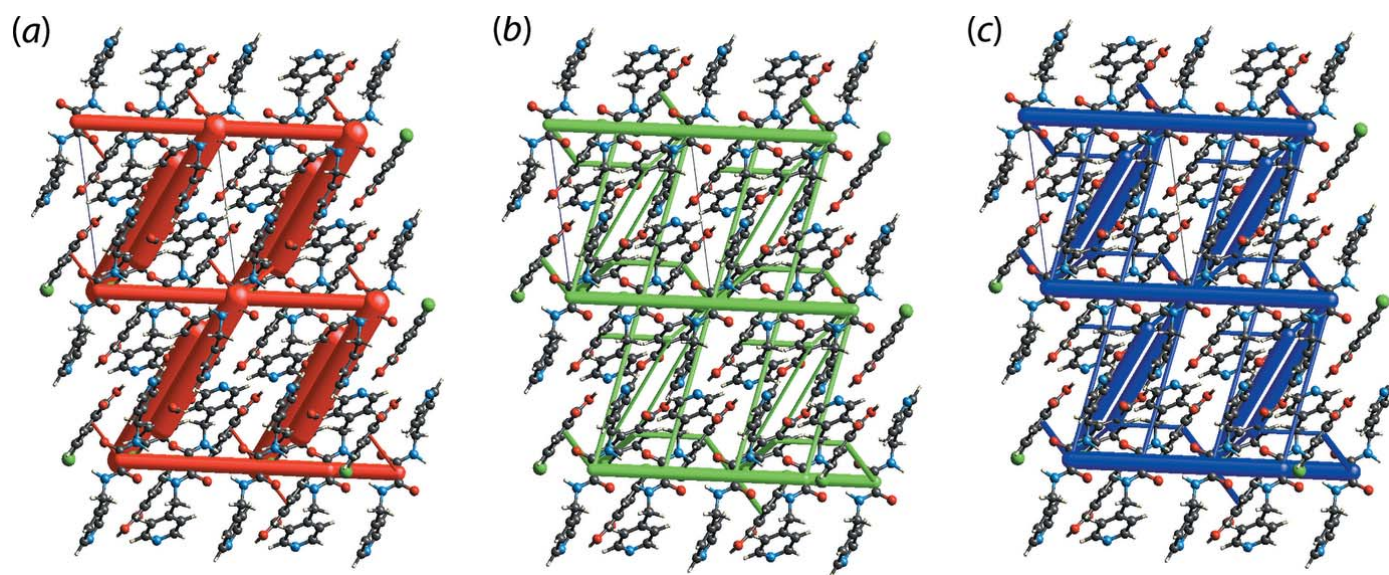

Figure 9
Perspective views of the energy frameworks of (I), showing the (a) electrostatic force, (b) dispersion force and (c) total energy. The radius of the cylinders is proportional to the relative strength of the corresponding energies and they were adjusted to the same scale factor of 100 with a cut-off value of 8 kJ mol^{-1} within a 2 × 2 × 2 unit cells.

Table 4
Experimental details.

Crystal data

Chemical formula	$C_{14}H_{14}N_4O_2 \cdot 2C_7H_5ClO_2$
M_r	583.41
Crystal system, space group	Triclinic, $P\bar{1}$
Temperature (K)	100
a, b, c (Å)	9.9401 (2), 11.2002 (2), 12.3308 (3)
α, β, γ (°)	78.871 (2), 78.816 (2), 81.992 (2)
V (Å³)	1313.98 (5)
Z	2
Radiation type	Cu $K\alpha$
μ (mm⁻¹)	2.67
Crystal size (mm)	$0.13 \times 0.04 \times 0.03$

Data collection

Diffractometer	XtaLAB Synergy, Dualflex, AtlasS2
Absorption correction	Gaussian (*CrysAlis PRO*; Rigaku OD, 2018)
T_{min}, T_{max}	0.847, 1.000
No. of measured, independent and observed [$I > 2\sigma(I)$] reflections	33133, 5486, 4814
R_{int}	0.034
$(\sin\theta/\lambda)_{max}$ (Å⁻¹)	0.631

Refinement

$R[F^2 > 2\sigma(F^2)]$, $wR(F^2)$, S	0.032, 0.090, 1.03
No. of reflections	5486
No. of parameters	373
No. of restraints	4
H-atom treatment	H atoms treated by a mixture of independent and constrained refinement
$\Delta\rho_{max}, \Delta\rho_{min}$ (e Å⁻³)	0.29, −0.33

Computer programs: *CrysAlis PRO* (Rigaku OD, 2018), *SHELXS* (Sheldrick, 2015a), *SHELXL2017* (Sheldrick, 2015b), *ORTEP-3 for Windows* (Farrugia, 2012), *DIAMOND* (Brandenburg, 2006) and *publCIF* (Westrip, 2010).

supramolecular architectures in co-crystals comprising $^4L\text{H}_2$ and multi-functional carboxylic acids.

7. Synthesis and crystallization

The precursor, N,N'-bis(pyridin-4-ylmethyl)oxalamide ($^4L\text{H}_2$) was prepared according to a literature procedure: m.p.: 486.3–487.6 K; lit. 486–487 K (Nguyen *et al.*, 1998). 4-Chlorobenzoic acid (Merck) was reagent grade and used as received without further purification. The co-former $^4L\text{H}_2$ (0.271 g, 0.001 mol) was mixed with 4-chlorobenzoic acid (0.157 g, 0.001 mol) and the mixture was then ground for 15 min in the presence of a few drops of methanol. The procedure was repeated twice. Colourless blocks were obtained through careful layering of toluene (1 ml) on an N,N-dimethylformamide (1 ml) solution of the ground mixture. M.p.: 456.9–458.6 K. IR (cm⁻¹): 3211 ν(N—H), 3052−2935 ν(C—H), 1669–1604 ν(C=O), 1492 ν(C=C), 1419 ν(C—N), 794 ν(C—Cl).

8. Refinement

Crystal data, data collection and structure refinement details are summarized in Table 4. The carbon-bound H atoms were placed in calculated positions (C—H = 0.95–0.99 Å) and were included in the refinement in the riding model approximation,

with U_{iso}(H) set to $1.2U_{eq}$(C). The oxygen- and nitrogen-bound H atoms were located from a difference-Fourier map and refined with O—H = 0.84±0.01 Å and N—H = 0.88±0.01 Å, respectively, and with U_{iso}(H) set to $1.5U_{eq}$(O) or $1.2U_{eq}$(N).

References

Arman, H. D., Kaulgud, T., Miller, T. & Tiekink, E. R. T. (2014). *Z. Kristallogr. Cryst. Mater.* **229**, 295–302.

Arman, H. D., Miller, T., Poplaukhin, P. & Tiekink, E. R. T. (2009). *Acta Cryst.* E**65**, o3178–o3179.

Arman, H. D., Miller, T., Poplaukhin, P. & Tiekink, E. R. T. (2013). *Zeitschrift Kristallogr.* **228**, 295–303.

Arman, H. D., Miller, T. & Tiekink, E. R. T. (2012). *Z. Kristallogr. Cryst. Mater.* **227**, 825–830.

Brandenburg, K. (2006). *DIAMOND*. Crystal Impact GbR, Bonn, Germany.

Chai, J. D. & Head-Gordon, M. (2008). *Phys. Chem. Chem. Phys.* **10**, 6615–6620.

Contreras-García, J., Johnson, E. R., Keinan, S., Chaudret, R., Piquemal, J.-P., Beratan, D. N. & Yang, W. (2011). *J. Chem. Theory Comput.* **7**, 625–632.

Etter, M. C. (1990). *Acc. Chem. Res.* **23**, 120–126.

Farrugia, L. J. (2012). *J. Appl. Cryst.* **45**, 849–854.

Frisch, M. J., *et al.* (2016). *Gaussian 16*, Revision A. 03. Gaussian, Inc., Wallingford CT, USA.

Johnson, E. R., Keinan, S., Mori-Sánchez, P., Contreras-García, J., Cohen, A. J. & Yang, W. (2010). *J. Am. Chem. Soc.* **132**, 6498–6506.

Jotani, M. M., Wardell, J. L. & Tiekink, E. R. T. (2019). *Z. Kristallogr.* **234**, 43–57.

Luong Nguyen, T., Scott, A., Dinkelmeyer, B., Fowler, F. W. & Lauher, J. W. (1998). *New J. Chem.* **22**, 129–135.

Nguyen, T. L., Fowler, F. W. & Lauher, J. W. (2001). *J. Am. Chem. Soc.* **123**, 11057–11064.

Petersson, G. A., Bennett, A., Tensfeldt, T. G., Al–Laham, M. A., Shirley, W. A. & Mantzaris, J. (1988). *J. Chem. Phys.* **89**, 2193–2218.

Rigaku OD (2018). *CrysAlis PRO* Software system. Rigaku Corporation, Oxford, UK.

Shattock, T. R., Arora, K. K., Vishweshwar, P. & Zaworotko, M. J. (2008). *Cryst. Growth Des.* **8**, 4533–4545.

Sheldrick, G. M. (2015a). *Acta Cryst.* A**71**, 3–8.

Sheldrick, G. M. (2015b). *Acta Cryst.* C**71**, 3–8.

Spackman, M. A. & Jayatilaka, D. (2009). *CrystEngComm*, **11**, 19–32.

Spek, A. L. (2020). *Acta Cryst.* E**76**, 1–11.

Syed, S., Jotani, M. M., Halim, S. N. A. & Tiekink, E. R. T. (2016). *Acta Cryst.* E**72**, 391–398.

Tan, S. L., Halcovitch, N. R. & Tiekink, E. R. T. (2019). *Acta Cryst.* E**75**, 1133–1139.

Tan, S. L., Jotani, M. M. & Tiekink, E. R. T. (2019). *Acta Cryst.* E**75**, 308–318.

Tan, S. L. & Tiekink, E. R. T. (2019). *Z. Kristallogr. New Cryst. Struct.* **234**, 1109–1111.

Tan, S. L. & Tiekink, E. R. T. (2020). *Acta Cryst.* E**76**, 102–110.

Tiekink, E. R. T. (2017). *Multi-Component Crystals: Synthesis, Concepts, Function*, edited by E. R. T. Tiekink & J. Schpector-Zukerman, pp. 289–319. Singapore: De Gruyter.

Turner, M. J., Mckinnon, J. J., Wolff, S. K., Grimwood, D. J., Spackman, P. R., Jayatilaka, D. & Spackman, M. A. (2017). Crystal Explorer 17. The University of Western Australia.

Westrip, S. P. (2010). *J. Appl. Cryst.* **43**, 920–925.

supporting information

Crystal structure, Hirshfeld surface analysis and computational study of the 1:2 co-crystal formed between *N,N′*-bis(pyridin-4-ylmethyl)ethanediamide and 4-chlorobenzoic acid

Sang Loon Tan and Edward R. T. Tiekink

Computing details

Data collection: *CrysAlis PRO* (Rigaku OD, 2018); cell refinement: *CrysAlis PRO* (Rigaku OD, 2018); data reduction: *CrysAlis PRO* (Rigaku OD, 2018); program(s) used to solve structure: *SHELXS* (Sheldrick, 2015*a*); program(s) used to refine structure: *SHELXL2017* (Sheldrick, 2015*b*); molecular graphics: *ORTEP-3 for Windows* (Farrugia, 2012), *DIAMOND* (Brandenburg, 2006); software used to prepare material for publication: *publCIF* (Westrip, 2010).

N,N′-**Bis(pyridin-4-ylmethyl)ethanediamide–4-chlorobenzoic acid (1/2)**

Crystal data

$C_{14}H_{14}N_4O_2 \cdot 2C_7H_5ClO_2$	$Z = 2$
$M_r = 583.41$	$F(000) = 604$
Triclinic, $P\overline{1}$	$D_x = 1.475$ Mg m^{-3}
$a = 9.9401$ (2) Å	Cu $K\alpha$ radiation, $\lambda = 1.54184$ Å
$b = 11.2002$ (2) Å	Cell parameters from 14644 reflections
$c = 12.3308$ (3) Å	$\theta = 3.7$–76.1°
$\alpha = 78.871$ (2)°	$\mu = 2.67$ mm^{-1}
$\beta = 78.816$ (2)°	$T = 100$ K
$\gamma = 81.992$ (2)°	Plate, colourless
$V = 1313.98$ (5) Å^3	$0.13 \times 0.04 \times 0.03$ mm

Data collection

XtaLAB Synergy, Dualflex, AtlasS2 diffractometer	33133 measured reflections
	5486 independent reflections
Radiation source: micro-focus sealed X-ray tube	4814 reflections with $I > 2\sigma(I)$
Detector resolution: 5.2558 pixels mm^{-1}	$R_{int} = 0.034$
ω scans	$\theta_{max} = 76.5°$, $\theta_{min} = 3.7°$
Absorption correction: gaussian	$h = -9 \rightarrow 12$
(CrysAlis PRO; Rigaku OD, 2018)	$k = -14 \rightarrow 14$
$T_{min} = 0.847$, $T_{max} = 1.000$	$l = -15 \rightarrow 15$

Refinement

Refinement on F^2	4 restraints
Least-squares matrix: full	Primary atom site location: structure-invariant direct methods
$R[F^2 > 2\sigma(F^2)] = 0.032$	
$wR(F^2) = 0.090$	Secondary atom site location: difference Fourier map
$S = 1.03$	
5486 reflections	Hydrogen site location: mixed
373 parameters	

H atoms treated by a mixture of independent and constrained refinement	$(\Delta/\sigma)_{max} = 0.002$		
$w = 1/[\sigma^2(F_o^2) + (0.0502P)^2 + 0.3813P]$ where $P = (F_o^2 + 2F_c^2)/3$	$\Delta\rho_{max} = 0.29$ e Å^{-3} $\Delta\rho_{min} = -0.33$ e Å^{-3}		

Special details

Geometry. All esds (except the esd in the dihedral angle between two l.s. planes) are estimated using the full covariance matrix. The cell esds are taken into account individually in the estimation of esds in distances, angles and torsion angles; correlations between esds in cell parameters are only used when they are defined by crystal symmetry. An approximate (isotropic) treatment of cell esds is used for estimating esds involving l.s. planes.

Fractional atomic coordinates and isotropic or equivalent isotropic displacement parameters (Å²)

	x	y	z	$U_{iso}*/U_{eq}$
O1	0.60739 (8)	0.97776 (8)	0.10123 (7)	0.01871 (18)
N1	0.18629 (11)	0.75161 (10)	0.46595 (9)	0.0226 (2)
N2	0.37710 (10)	1.03739 (10)	0.11754 (9)	0.0171 (2)
H2N	0.3042 (12)	1.0441 (15)	0.0858 (13)	0.021*
C1	0.10938 (13)	0.85755 (12)	0.43978 (11)	0.0219 (3)
H1	0.014870	0.864969	0.473525	0.026*
C2	0.16098 (12)	0.95678 (12)	0.36591 (11)	0.0200 (2)
H2	0.102752	1.030329	0.349550	0.024*
C3	0.29944 (12)	0.94745 (11)	0.31582 (10)	0.0179 (2)
C4	0.38016 (13)	0.83804 (12)	0.34405 (11)	0.0213 (3)
H4	0.475365	0.828721	0.312628	0.026*
C5	0.32023 (13)	0.74264 (12)	0.41854 (11)	0.0235 (3)
H5	0.376045	0.668080	0.436755	0.028*
C6	0.35802 (12)	1.05429 (12)	0.23434 (11)	0.0197 (2)
H6A	0.295105	1.129610	0.244075	0.024*
H6B	0.447977	1.065548	0.251964	0.024*
C7	0.50027 (11)	1.00274 (10)	0.06174 (10)	0.0146 (2)
O2	1.10206 (8)	0.99617 (8)	0.10296 (7)	0.02007 (19)
N3	0.69677 (11)	0.75172 (10)	0.47531 (9)	0.0211 (2)
N4	0.86920 (10)	1.03345 (10)	0.11304 (9)	0.0173 (2)
H4N	0.8027 (13)	1.0328 (15)	0.0771 (12)	0.021*
C8	0.65934 (13)	0.86787 (12)	0.49045 (11)	0.0216 (3)
H8	0.599965	0.882524	0.557915	0.026*
C9	0.70303 (12)	0.96737 (12)	0.41257 (11)	0.0202 (2)
H9	0.674340	1.048201	0.426901	0.024*
C10	0.78943 (11)	0.94780 (11)	0.31302 (10)	0.0174 (2)
C11	0.82958 (12)	0.82740 (12)	0.29757 (11)	0.0210 (3)
H11	0.889290	0.810106	0.231079	0.025*
C12	0.78155 (13)	0.73269 (12)	0.38030 (11)	0.0221 (3)
H12	0.810108	0.650822	0.368968	0.027*
C13	0.83531 (12)	1.05668 (11)	0.22714 (10)	0.0186 (2)
H13A	0.760868	1.125137	0.231071	0.022*
H13B	0.917196	1.082945	0.246930	0.022*
C14	0.99697 (11)	1.00732 (11)	0.06123 (10)	0.0154 (2)
Cl1	−0.37720 (3)	0.26656 (3)	1.00591 (3)	0.02890 (10)

O3	−0.07627 (10)	0.73883 (9)	0.67521 (9)	0.0304 (2)
O4	0.03544 (10)	0.58218 (9)	0.59372 (8)	0.0268 (2)
H4O	0.0841 (18)	0.6388 (14)	0.5594 (16)	0.040*
C15	−0.06010 (13)	0.63083 (12)	0.66763 (11)	0.0222 (3)
C16	−0.14493 (12)	0.53923 (12)	0.74585 (11)	0.0205 (3)
C17	−0.23844 (13)	0.57765 (12)	0.83541 (11)	0.0216 (3)
H17	−0.252419	0.661813	0.841895	0.026*
C18	−0.31121 (13)	0.49417 (12)	0.91512 (11)	0.0220 (3)
H18	−0.374727	0.520178	0.976363	0.026*
C19	−0.28935 (13)	0.37174 (12)	0.90357 (12)	0.0217 (3)
C20	−0.19944 (13)	0.33124 (12)	0.81370 (12)	0.0240 (3)
H20	−0.187517	0.247331	0.806467	0.029*
C21	−0.12741 (13)	0.41610 (12)	0.73471 (12)	0.0230 (3)
H21	−0.065666	0.390163	0.672537	0.028*
Cl2	0.09083 (4)	0.27800 (3)	0.98266 (3)	0.03057 (10)
O5	0.42589 (10)	0.74219 (9)	0.67193 (9)	0.0298 (2)
O6	0.56489 (9)	0.58098 (9)	0.61812 (8)	0.0242 (2)
H6O	0.6094 (17)	0.6374 (14)	0.5776 (14)	0.036*
C22	0.45469 (13)	0.63220 (12)	0.67727 (11)	0.0205 (3)
C23	0.36560 (12)	0.54182 (12)	0.75218 (11)	0.0194 (2)
C24	0.22992 (13)	0.58221 (12)	0.79557 (11)	0.0221 (3)
H24	0.196233	0.665934	0.777238	0.026*
C25	0.14420 (13)	0.50108 (12)	0.86510 (11)	0.0227 (3)
H25	0.051448	0.527996	0.893646	0.027*
C26	0.19648 (14)	0.37974 (12)	0.89221 (11)	0.0223 (3)
C27	0.33072 (14)	0.33723 (12)	0.85065 (12)	0.0237 (3)
H27	0.364433	0.253713	0.870218	0.028*
C28	0.41476 (13)	0.41920 (12)	0.77991 (11)	0.0212 (3)
H28	0.506744	0.391414	0.750081	0.025*

Atomic displacement parameters (Å²)

	U^{11}	U^{22}	U^{33}	U^{12}	U^{13}	U^{23}
O1	0.0124 (4)	0.0244 (4)	0.0184 (4)	−0.0031 (3)	−0.0020 (3)	−0.0012 (3)
N1	0.0252 (5)	0.0229 (6)	0.0182 (5)	−0.0028 (4)	0.0006 (4)	−0.0039 (4)
N2	0.0126 (4)	0.0213 (5)	0.0165 (5)	−0.0018 (4)	−0.0001 (4)	−0.0036 (4)
C1	0.0181 (5)	0.0265 (7)	0.0199 (6)	−0.0024 (5)	0.0006 (5)	−0.0049 (5)
C2	0.0179 (6)	0.0229 (6)	0.0181 (6)	0.0003 (5)	−0.0019 (5)	−0.0041 (5)
C3	0.0184 (5)	0.0217 (6)	0.0145 (5)	−0.0025 (4)	−0.0016 (4)	−0.0063 (5)
C4	0.0189 (6)	0.0246 (6)	0.0192 (6)	0.0007 (5)	−0.0001 (5)	−0.0062 (5)
C5	0.0256 (6)	0.0223 (6)	0.0202 (6)	0.0029 (5)	−0.0018 (5)	−0.0041 (5)
C6	0.0198 (6)	0.0208 (6)	0.0179 (6)	−0.0033 (5)	0.0015 (5)	−0.0061 (5)
C7	0.0134 (5)	0.0125 (5)	0.0166 (6)	−0.0038 (4)	−0.0002 (4)	0.0002 (4)
O2	0.0128 (4)	0.0279 (5)	0.0189 (4)	−0.0032 (3)	−0.0018 (3)	−0.0028 (4)
N3	0.0195 (5)	0.0227 (5)	0.0200 (5)	−0.0023 (4)	−0.0010 (4)	−0.0031 (4)
N4	0.0118 (4)	0.0227 (5)	0.0168 (5)	−0.0019 (4)	−0.0011 (4)	−0.0036 (4)
C8	0.0219 (6)	0.0249 (6)	0.0179 (6)	−0.0028 (5)	0.0006 (5)	−0.0069 (5)
C9	0.0196 (6)	0.0207 (6)	0.0202 (6)	−0.0014 (5)	−0.0001 (5)	−0.0070 (5)

C10	0.0124 (5)	0.0220 (6)	0.0185 (6)	−0.0020 (4)	−0.0026 (4)	−0.0047 (5)
C11	0.0179 (5)	0.0227 (6)	0.0205 (6)	−0.0003 (5)	0.0024 (5)	−0.0062 (5)
C12	0.0202 (6)	0.0199 (6)	0.0247 (7)	−0.0001 (5)	0.0004 (5)	−0.0057 (5)
C13	0.0161 (5)	0.0202 (6)	0.0184 (6)	−0.0020 (4)	0.0015 (4)	−0.0053 (5)
C14	0.0134 (5)	0.0142 (5)	0.0171 (6)	−0.0036 (4)	−0.0005 (4)	0.0003 (4)
Cl1	0.02788 (17)	0.02064 (16)	0.03483 (19)	−0.00701 (12)	−0.00165 (13)	0.00283 (13)
O3	0.0325 (5)	0.0191 (5)	0.0334 (6)	−0.0029 (4)	0.0071 (4)	−0.0023 (4)
O4	0.0290 (5)	0.0232 (5)	0.0250 (5)	−0.0049 (4)	0.0060 (4)	−0.0053 (4)
C15	0.0219 (6)	0.0215 (6)	0.0221 (6)	−0.0008 (5)	−0.0026 (5)	−0.0030 (5)
C16	0.0186 (5)	0.0205 (6)	0.0224 (6)	−0.0020 (5)	−0.0038 (5)	−0.0037 (5)
C17	0.0223 (6)	0.0171 (6)	0.0252 (7)	−0.0015 (5)	−0.0034 (5)	−0.0043 (5)
C18	0.0204 (6)	0.0213 (6)	0.0237 (6)	−0.0029 (5)	−0.0012 (5)	−0.0045 (5)
C19	0.0186 (5)	0.0195 (6)	0.0268 (7)	−0.0047 (5)	−0.0052 (5)	−0.0005 (5)
C20	0.0220 (6)	0.0174 (6)	0.0337 (7)	−0.0016 (5)	−0.0057 (5)	−0.0065 (5)
C21	0.0202 (6)	0.0228 (6)	0.0265 (7)	−0.0012 (5)	−0.0026 (5)	−0.0078 (5)
Cl2	0.03914 (19)	0.02243 (17)	0.02819 (18)	−0.01267 (13)	0.00685 (14)	−0.00548 (13)
O5	0.0297 (5)	0.0185 (5)	0.0339 (6)	−0.0007 (4)	0.0079 (4)	−0.0010 (4)
O6	0.0214 (4)	0.0210 (5)	0.0258 (5)	−0.0010 (4)	0.0039 (4)	−0.0023 (4)
C22	0.0199 (6)	0.0198 (6)	0.0206 (6)	−0.0004 (5)	−0.0027 (5)	−0.0027 (5)
C23	0.0199 (6)	0.0196 (6)	0.0184 (6)	−0.0018 (5)	−0.0025 (5)	−0.0037 (5)
C24	0.0218 (6)	0.0180 (6)	0.0247 (6)	0.0009 (5)	−0.0026 (5)	−0.0030 (5)
C25	0.0205 (6)	0.0233 (6)	0.0237 (6)	−0.0019 (5)	−0.0009 (5)	−0.0053 (5)
C26	0.0272 (6)	0.0207 (6)	0.0196 (6)	−0.0073 (5)	−0.0007 (5)	−0.0046 (5)
C27	0.0298 (7)	0.0167 (6)	0.0238 (6)	−0.0007 (5)	−0.0029 (5)	−0.0039 (5)
C28	0.0214 (6)	0.0200 (6)	0.0216 (6)	0.0010 (5)	−0.0022 (5)	−0.0059 (5)

Geometric parameters (Å, º)

O1—C7	1.2307 (14)	C13—H13A	0.9900
N1—C1	1.3386 (17)	C13—H13B	0.9900
N1—C5	1.3445 (17)	C14—C14ii	1.539 (2)
N2—C7	1.3292 (15)	Cl1—C19	1.7402 (13)
N2—C6	1.4612 (16)	O3—C15	1.2172 (17)
N2—H2N	0.876 (9)	O4—C15	1.3196 (16)
C1—C2	1.3838 (19)	O4—H4O	0.847 (9)
C1—H1	0.9500	C15—C16	1.4958 (18)
C2—C3	1.3935 (17)	C16—C17	1.3938 (19)
C2—H2	0.9500	C16—C21	1.3957 (18)
C3—C4	1.3915 (18)	C17—C18	1.3861 (19)
C3—C6	1.5111 (17)	C17—H17	0.9500
C4—C5	1.3879 (19)	C18—C19	1.3886 (19)
C4—H4	0.9500	C18—H18	0.9500
C5—H5	0.9500	C19—C20	1.389 (2)
C6—H6A	0.9900	C20—C21	1.388 (2)
C6—H6B	0.9900	C20—H20	0.9500
C7—C7i	1.537 (2)	C21—H21	0.9500
O2—C14	1.2325 (14)	Cl2—C26	1.7418 (13)
N3—C12	1.3385 (17)	O5—C22	1.2173 (17)

N3—C8	1.3408 (17)	O6—C22	1.3181 (16)
N4—C14	1.3269 (15)	O6—H6O	0.846 (9)
N4—C13	1.4471 (16)	C22—C23	1.4945 (18)
N4—H4N	0.865 (9)	C23—C28	1.3923 (18)
C8—C9	1.3830 (19)	C23—C24	1.3977 (17)
C8—H8	0.9500	C24—C25	1.3850 (19)
C9—C10	1.3911 (17)	C24—H24	0.9500
C9—H9	0.9500	C25—C26	1.3871 (19)
C10—C11	1.3906 (18)	C25—H25	0.9500
C10—C13	1.5118 (17)	C26—C27	1.3862 (19)
C11—C12	1.3886 (19)	C27—C28	1.3869 (19)
C11—H11	0.9500	C27—H27	0.9500
C12—H12	0.9500	C28—H28	0.9500
C1—N1—C5	117.89 (11)	N4—C13—H13B	108.7
C7—N2—C6	121.67 (10)	C10—C13—H13B	108.7
C7—N2—H2N	119.5 (11)	H13A—C13—H13B	107.6
C6—N2—H2N	118.6 (11)	O2—C14—N4	125.67 (11)
N1—C1—C2	123.12 (12)	O2—C14—C14ii	121.76 (13)
N1—C1—H1	118.4	N4—C14—C14ii	112.57 (12)
C2—C1—H1	118.4	C15—O4—H4O	106.4 (14)
C1—C2—C3	119.15 (12)	O3—C15—O4	124.16 (12)
C1—C2—H2	120.4	O3—C15—C16	122.31 (12)
C3—C2—H2	120.4	O4—C15—C16	113.49 (11)
C4—C3—C2	117.87 (12)	C17—C16—C21	119.62 (12)
C4—C3—C6	121.98 (11)	C17—C16—C15	118.56 (12)
C2—C3—C6	120.14 (11)	C21—C16—C15	121.73 (12)
C5—C4—C3	119.37 (11)	C18—C17—C16	120.60 (12)
C5—C4—H4	120.3	C18—C17—H17	119.7
C3—C4—H4	120.3	C16—C17—H17	119.7
N1—C5—C4	122.59 (12)	C17—C18—C19	118.62 (12)
N1—C5—H5	118.7	C17—C18—H18	120.7
C4—C5—H5	118.7	C19—C18—H18	120.7
N2—C6—C3	112.69 (10)	C18—C19—C20	122.06 (12)
N2—C6—H6A	109.1	C18—C19—Cl1	118.50 (10)
C3—C6—H6A	109.1	C20—C19—Cl1	119.44 (10)
N2—C6—H6B	109.1	C21—C20—C19	118.52 (12)
C3—C6—H6B	109.1	C21—C20—H20	120.7
H6A—C6—H6B	107.8	C19—C20—H20	120.7
O1—C7—N2	125.33 (11)	C20—C21—C16	120.55 (12)
O1—C7—C7i	121.12 (13)	C20—C21—H21	119.7
N2—C7—C7i	113.55 (12)	C16—C21—H21	119.7
C12—N3—C8	117.64 (11)	C22—O6—H6O	108.1 (13)
C14—N4—C13	123.73 (10)	O5—C22—O6	124.16 (12)
C14—N4—H4N	117.5 (11)	O5—C22—C23	122.35 (12)
C13—N4—H4N	118.7 (11)	O6—C22—C23	113.49 (11)
N3—C8—C9	123.14 (12)	C28—C23—C24	119.54 (12)
N3—C8—H8	118.4	C28—C23—C22	121.62 (11)

C9—C8—H8	118.4	C24—C23—C22	118.84 (11)
C8—C9—C10	119.28 (12)	C25—C24—C23	120.48 (12)
C8—C9—H9	120.4	C25—C24—H24	119.8
C10—C9—H9	120.4	C23—C24—H24	119.8
C11—C10—C9	117.71 (12)	C24—C25—C26	118.68 (12)
C11—C10—C13	123.06 (11)	C24—C25—H25	120.7
C9—C10—C13	119.23 (11)	C26—C25—H25	120.7
C12—C11—C10	119.35 (12)	C27—C26—C25	122.06 (12)
C12—C11—H11	120.3	C27—C26—Cl2	118.96 (10)
C10—C11—H11	120.3	C25—C26—Cl2	118.97 (10)
N3—C12—C11	122.87 (12)	C26—C27—C28	118.61 (12)
N3—C12—H12	118.6	C26—C27—H27	120.7
C11—C12—H12	118.6	C28—C27—H27	120.7
N4—C13—C10	114.16 (10)	C27—C28—C23	120.62 (12)
N4—C13—H13A	108.7	C27—C28—H28	119.7
C10—C13—H13A	108.7	C23—C28—H28	119.7
C5—N1—C1—C2	0.7 (2)	O4—C15—C16—C17	172.82 (12)
N1—C1—C2—C3	−0.1 (2)	O3—C15—C16—C21	178.55 (13)
C1—C2—C3—C4	−0.79 (18)	O4—C15—C16—C21	−3.73 (18)
C1—C2—C3—C6	179.63 (11)	C21—C16—C17—C18	1.81 (19)
C2—C3—C4—C5	1.09 (18)	C15—C16—C17—C18	−174.81 (12)
C6—C3—C4—C5	−179.34 (12)	C16—C17—C18—C19	−0.24 (19)
C1—N1—C5—C4	−0.3 (2)	C17—C18—C19—C20	−1.41 (19)
C3—C4—C5—N1	−0.5 (2)	C17—C18—C19—Cl1	178.20 (10)
C7—N2—C6—C3	−101.17 (13)	C18—C19—C20—C21	1.4 (2)
C4—C3—C6—N2	76.87 (14)	Cl1—C19—C20—C21	−178.18 (10)
C2—C3—C6—N2	−103.57 (13)	C19—C20—C21—C16	0.20 (19)
C6—N2—C7—O1	2.55 (18)	C17—C16—C21—C20	−1.79 (19)
C6—N2—C7—C7ⁱ	−176.74 (11)	C15—C16—C21—C20	174.72 (12)
C12—N3—C8—C9	0.65 (19)	O5—C22—C23—C28	−163.13 (13)
N3—C8—C9—C10	0.33 (19)	O6—C22—C23—C28	17.41 (17)
C8—C9—C10—C11	−0.96 (18)	O5—C22—C23—C24	16.56 (19)
C8—C9—C10—C13	179.04 (11)	O6—C22—C23—C24	−162.89 (12)
C9—C10—C11—C12	0.65 (18)	C28—C23—C24—C25	−0.43 (19)
C13—C10—C11—C12	−179.36 (11)	C22—C23—C24—C25	179.87 (12)
C8—N3—C12—C11	−0.99 (19)	C23—C24—C25—C26	1.1 (2)
C10—C11—C12—N3	0.3 (2)	C24—C25—C26—C27	−0.9 (2)
C14—N4—C13—C10	−98.77 (13)	C24—C25—C26—Cl2	178.27 (10)
C11—C10—C13—N4	26.33 (16)	C25—C26—C27—C28	0.1 (2)
C9—C10—C13—N4	−153.67 (11)	Cl2—C26—C27—C28	−179.13 (10)
C13—N4—C14—O2	2.03 (19)	C26—C27—C28—C23	0.6 (2)
C13—N4—C14—C14ⁱⁱ	−177.41 (12)	C24—C23—C28—C27	−0.46 (19)
O3—C15—C16—C17	−4.90 (19)	C22—C23—C28—C27	179.24 (12)

Symmetry codes: (i) −*x*+1, −*y*+2, −*z*; (ii) −*x*+2, −*y*+2, −*z*.

Hydrogen-bond geometry (Å, º)

D—H···A	D—H	H···A	D···A	D—H···A
N2—H2*N*···O1[i]	0.88 (1)	2.35 (2)	2.7088 (14)	105 (1)
N4—H4*N*···O2[ii]	0.87 (1)	2.30 (2)	2.7028 (14)	108 (1)
O4—H4*O*···N1	0.85 (2)	1.82 (2)	2.6559 (15)	171 (2)
O6—H6*O*···N3	0.85 (2)	1.80 (2)	2.6419 (15)	172 (2)
C8—H8···O5	0.95	2.53	3.1708 (17)	125
N2—H2*N*···O2[iii]	0.88 (1)	2.11 (1)	2.8800 (13)	146 (1)
N4—H4*N*···O1	0.87 (1)	2.07 (1)	2.7959 (13)	141 (1)
C2—H2···O3[iv]	0.95	2.53	3.3597 (17)	146
C6—H6*A*···O3[iv]	0.99	2.59	3.5262 (17)	157
C9—H9···O5[v]	0.95	2.59	3.3701 (17)	140
C13—H13*A*···O5[v]	0.99	2.48	3.4006 (16)	155
C27—H27···O1[vi]	0.95	2.53	3.4505 (16)	163

Symmetry codes: (i) −*x*+1, −*y*+2, −*z*; (ii) −*x*+2, −*y*+2, −*z*; (iii) *x*−1, *y*, *z*; (iv) −*x*, −*y*+2, −*z*+1; (v) −*x*+1, −*y*+2, −*z*+1; (vi) −*x*+1, −*y*+1, −*z*+1.